Generation of Subnatural-Linewidth Hyperentangled Photon Pairs

Kaiyu Liao,[1] Hui Yan,[1,*] Junyu He,[1] Shengwang Du,[2] Zhi-Ming Zhang,[3] and Shi-Liang Zhu[4,1,†]

[1]*Laboratory of Quantum Engineering and Quantum Materials, School of Physics and Telecommunication Engineering, South China Normal University, Guangzhou 510006, China*

[2]*Department of Physics, The Hong Kong University of Science and Technology, Clear Water Bay, Kowloon, Hong Kong, China*

[3]*Laboratory of Quantum Engineering and Quantum Materials, School of Information and Photoelectronic Science and Engineering, South China Normal University, Guangzhou 510006, China*

[4]*National Laboratory of Solid State Microstructures, School of Physics, Nanjing University, Nanjing 210093, China*

arXiv:1402.2530v1 [quant-ph] 11 Feb 2014

We demonstrate an efficient experimental scheme for producing hyperentangled photon pairs from spontaneous four-wave mixing (SFWM) in a laser cooled ^{85}Rb atomic ensemble, with a bandwidth (as low as 0.8 MHz) much narrower than the rubidium atomic natural linewidth. The time-frequency entanglement of the photons results from the energy conservation of the continuous wave SFWM processes. We make use of a Mach-Zehnder interferometer configuration to entangle their polarization states. By stabilizing the relative phase between the two SFWM paths, we are able to produce all four Bell states. These subnatural linewidth photon pairs with both time-frequency and polarization entanglements are ideal quantum information carriers for connecting remote atomic quantum nodes via efficient light-matter interaction in a photon-atom quantum network.

PACS numbers: 42.50.Dv,03.67.Bg,42.65.Lm

The connectivity of a long-distance photon-atom quantum network strongly depends on efficient interactions between flying photonic quantum bits and local long-lived atomic matter nodes [1, 2]. Such efficient quantum interfaces, which convert quantum states (such as time-frequency waveform and polarizations) between photons and atoms, require the photons have a bandwidth sufficiently narrower than the natural linewidth of related atomic transitions (such as 6 MHz for rubidium D1 and D2 lines). Hyperentangled photon pairs, with entanglement in more than one degree of freedom, are particularly promising due to their high information capacity [3–5]. As a standard method for producing entangled photons, spontaneous parametric down conversion in a nonlinear crystal usually has a wide bandwidth (> THz) and very short coherence time (< ps). Many efforts have been investigated in the past more than one decade to narrow down the spontaneous parametric down conversion photon bandwidth using optical cavities to about 10 MHz [6–8], which is still wider than most atomic transitions and leads to a very low efficiency of storing these photons in a quantum memory [9].

Our motivation was stimulated by the recent progress in generating subnatural linewidth biphotons using continuous-wave spontaneous four-wave mixing (SFWM) in a laser cooled atomic ensemble with electromagnetically induced transparency (EIT) [10, 11]. Photons produced from this method not only have narrow bandwidth but also automatically match the atomic transitions. The applications of these narrow-band photons include the demonstration of a single-photon memory with a storage efficiency of about 50% [12], single photon precursor [13], and coherent control of single-photon absorption and reemission [14]. However, while this method provides a natural entanglement mechanism in the time-frequency domain, it is extremely difficult to produce polarization entanglement because of the polarization selectivity of EIT in a non-polarized atomic medium [15]. It is possible to generate the polarization entanglement by scarifying the EIT effect, but the photon generation efficiency is low and the bandwidth is not narrower than the atomic natural linewidth [16]. The "writing-reading" technique with optical pumping provides a solution to polarization entanglement but results in reducing time-frequency entanglement [17].

In this Letter, we report our work on producing subnatural linewidth hyperentangled photon pairs using the continuous-wave SFWM cold-atom EIT configuration. We demonstrate that the polarization entanglement can be efficiently produced by making use of a Mach-Zehnder interferometer in a two-path SFWM setup while maintaining the EIT effect in controlling the photon bandwidth and the time-frequency entanglement. By tuning the phase difference between the two SFWM paths and properly setting the driving laser polarizations, we can generate all four Bell states. These photons have coherence time of up to 900 ns and an estimated bandwidth of about 1 MHz that is much narrower than the Rb atomic natural linewidth (6 MHz). These subnatural linewidth, time-frequency and polarization entangled photon pairs are ideal flying qubits for connecting remote atomic quantum nodes in a quantum network.

Our experimental setup is illustrated in Fig. 1. We work with a two-dimensional ^{85}Rb magneto-optical trap (MOT) with a longitudinal length of $L = 1.7$ cm [18]. The experiment is run periodically. In each cycle, after

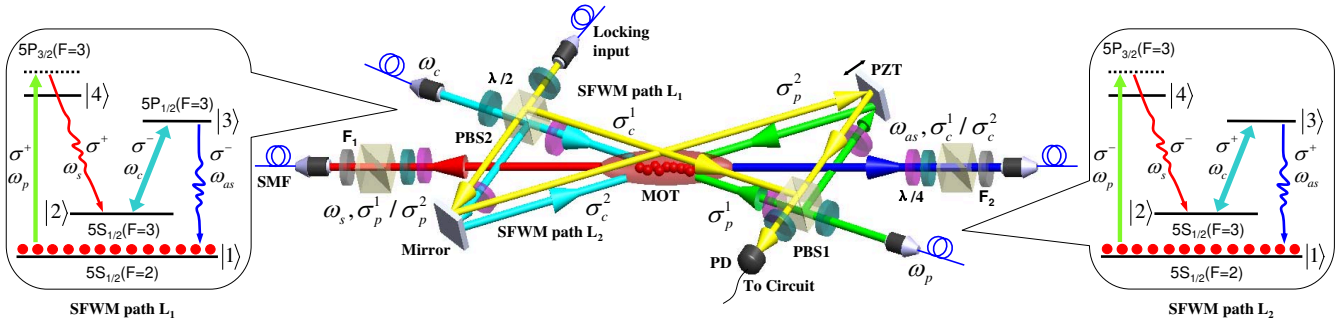

FIG. 1: (color online). Experimental setup for producing entangled photon pairs. The polarization entanglement is created by the quantum interference of the two spatially symmetric SFWM processes driven by two counter-propagating pump-coupling beams (L_1 and L_2). The phase difference of the two SFWM paths is stabilized by locking the reference laser Mach-Zehnder interferometer, whose output is detected by a photo detector (PD). To avoid its interaction with the cold atoms, the reference beams are slightly shifted away from the pump-coupling beams but pass through the same optical components. The inserted energy level diagrams are two possible SFWM channels for L_1 and L_2, respectively. PZT: Piezoe-lectric Transducer.

4.5 ms MOT time, the atoms are prepared in the ground level $|1\rangle$ and followed by 0.5 ms SFWM biphoton generation window. Along the longitudinal direction, the atoms have an optical depth of 32 in the $|1\rangle \rightarrow |3\rangle$ transition. The pump laser (780 nm, ω_p) is 80 MHz blue detuned from the transition $|1\rangle \rightarrow |4\rangle$, and the coupling laser (795 nm, ω_c) is on resonance with the transition $|2\rangle \rightarrow |3\rangle$. The linear polarized pump laser beam, with a $1/e^2$ diameter of 1.8 mm, is equally split into two beams after a half-wave plate and the first polarization beam splitter (PBS1). These two beams, with opposite circular polarizations (σ^+ and σ^-) after two quarter-wave plates, then intersect at the MOT with an angle of $\pm 2.5°$ to the longitudinal axis. Similarly, the two coupling laser beams after PBS2 with opposite circular polarizations overlap with the two pump beams from opposite directions. In presence of these two pairs of counter-propagating pump-coupling beams, phase-matched Stokes (ω_s) and anti-Stokes (ω_{as}) paired photons are produced along the longitudinal axis and coupled into two opposing single-mode fibers (SMF). In each SFWM path, the polarizations of the Stokes and anti-Stokes photons follow these of the corresponding pump and coupling field, respectively. The two SMF spatial modes are focused at the MOT center with a $1/e^2$ diameter of 0.4 mm. After two narrowband filters (F_1 and F_2, 0.5 GHz bandwidth), the photons are detected by two single-photon counter modules (SPCM, Perkin Elmer SPCM-4Q4C) and analyzed by a time-to-digital converter (Fast Comtec P7888) with a time bin width of 1 ns. Two sets of quarter-wave plates, half-wave plates, and PBSs are inserted for measuring polarization correlation and quantum state tomography.

To obtain the polarization entanglement, we must stabilize the phase difference between the two SFWM spatial paths. This is achieved by injecting a reference laser beam (795 nm, 110 MHz blue detuned from the transition $|2\rangle \rightarrow |3\rangle$) from the second input of PBS2. The two reference beams split after PBS2 are then recombined after PBS1 and detected by a photo detector (PD, a half wave plate and a PBS are used to obtain the interference), as shown in Fig. 1. This is a standard Mach-Zehnder interferometer to the reference laser. Locking the phase difference of the two arms of the Mach-Zehnder interferometer with a feedback electronics stabilizes the phase of the two SFWM paths [See the supplementary material [19]]. To avoid its interaction with the cold atoms, the reference beams are slightly shifted away from the pump-coupling beams but pass through the same optical components.

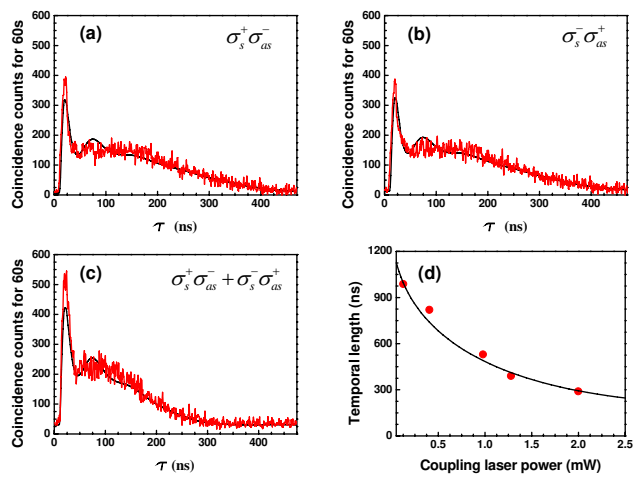

FIG. 2: (color online). (a,b,c) Two-photon coincidence counts as a function of the relative time delay between the Stokes and anti-Stokes photons: (a) Path 1: $\sigma_p^1 = \sigma^+$ and $\sigma_c^1 = \sigma^-$, Path 2: blocked; (b) Path 1: blocked, Path 2: $\sigma_p^2 = \sigma^-$ and $\sigma_c^2 = \sigma^+$; (c) Both paths are present. (d) The temporal length of the paired photons as a function of the coupling laser power. All the black lines are theoretically fitted.

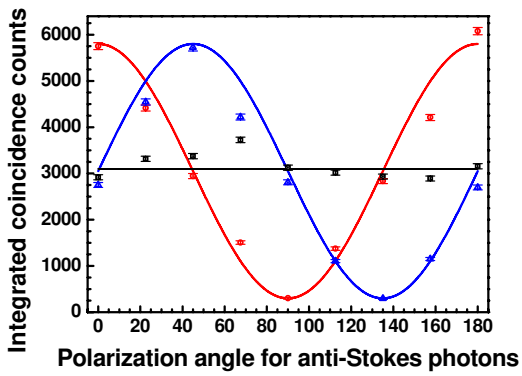

FIG. 3: (color online). Polarization correlation of the paired Stokes and anti-Stokes photons at ϕ=0. The polarization angle for Stokes photons are set at 0° (red line and circle) and −45° (blue line and triangle). The black squares are the data taken without stabilizing ϕ.

Following the perturbation theory [11], the produced two-photon state can be described as [See the supplemental material [19] for the derivation]

$$|\Psi\rangle = L\int \kappa(\omega_{as})\mathrm{sinc}[\frac{\Delta k(\omega_{as})L}{2}]|\omega_s=\omega_p+\omega_c-\omega_{as}\rangle |\omega_{as}\rangle d\omega_{as}\otimes\frac{1}{\sqrt{2}}(|\sigma_p^1\rangle_s|\sigma_c^1\rangle_{as}+e^{i\phi}|\sigma_p^2\rangle_s|\sigma_c^2\rangle_{as}), \quad (1)$$

which shows hyper-entanglement in frequency (continuous) and polarization (discrete). The upper indices (1 and 2) represent the two SFWM spatial paths. $\Delta k(\omega_{as})$ is the phase mismatching, and $\kappa(\omega_{as})$ is the nonlinear parametric coupling coefficient. $\kappa(\omega_{as})\mathrm{sinc}[\frac{\Delta k(\omega_{as})L}{2}]$ determines the photon spectrum. ϕ is the phase difference between the two SFWM paths. Equation (1) can also be rewritten in the time and polarization domains

$$|\Psi(t_s,t_{as})\rangle = \psi(t_{as}-t_s)e^{-i(\overline{\omega}_{as}t_{as}+\overline{\omega}_s t_s)} \otimes\frac{1}{\sqrt{2}}(|\sigma_p^1\rangle_s|\sigma_c^1\rangle_{as}+e^{i\phi}|\sigma_p^2\rangle_s|\sigma_c^2\rangle_{as}), \quad (2)$$

where t_s and t_{as} are the detection time of the Stokes and anti-Stokes photons, respectively. $\overline{\omega}_s$ and $\overline{\omega}_{as}$ are their central frequencies, respectively. The time-domain wave function $\psi(t_{as}-t_s)$ results from the frequency entanglement ($\omega_s=\omega_p+\omega_c-\omega_{as}$) and is the Fourier transform of the two-photon joint spectrum. Meanwhile, as shown in Eqs. (1) and (2), the polarization entanglement can be manipulated by controlling the pump-coupling polarizations and phase difference.

We first characterize the two-photon nonclassical correlation in time domain. Figure 2 (a)-(c) show the two-photon coincidence counts as functions of relative time delay ($\tau = t_{as}-t_s$) with the polarization configurations $\sigma_s^+\sigma_{as}^-$, $\sigma_s^-\sigma_{as}^+$, and $\sigma_s^+\sigma_{as}^- + \sigma_s^-\sigma_{as}^+$, respectively. We carefully balance the pump and coupling laser powers on the two SFWM paths to make their correlation indistinguishable in time domain for achieving the maximally polarization entangled states. At each path, the pump beam has a power of 35 μW and the coupling beam of 2 mW. Normalizing the coincidence counts to the accidental uncorrelated background counts, we obtain the normalized cross-correlation $g^{(2)}_{s,as}(\tau)$ with a peak value of 14 at τ=25 ns. With measured auto-correlations $g^{(2)}_{s,s}(0) = g^{(2)}_{as,as}(0) \approx 2.0$, we confirm that the Cauchy-Schwartz inequality $[g^{(2)}_{s,as}(\tau)]^2 \leq g^{(2)}_{s,s}(0)g^{(2)}_{as,as}(0)$ is violated by a factor of 49, which clearly indicates the quantum nature of the paired photons. The solid curves in Fig. 2(a)-(c) are calculated from Eq. (2). The nearly perfect agreement between the theory and experiment indirectly verifies the time-frequency entanglement. The shorter correlation time in Fig. 2(c) compared to that in Fig.2(a) and (b) are caused by the addition of the powers from the two coupling beams that widen the EIT and biphoton bandwidth. The coherence time of about 300 ns corresponds to an estimated bandwidth of 2.9 MHz (also confirmed from the theory). The photon bandwidth can be further reduced by lowering the coupling laser power to narrow the EIT window. Figure 2(d) shows the measured correlation time vs the coupling laser power. With 0.13 mW coupling laser power, we obtain a coherence time of up to 900 ns, which corresponds to a bandwidth of about 0.8 MHz. The solid curve in Fig. 2(d) is also obtained with Eq. (2).

We next demonstrate that all four polarization-entangled Bell states can be realized by locking the phase ϕ as well as properly choosing the polarizations of the coupling and pump laser beams. As shown in Eq. (2), locking the phase difference ϕ as 0 or π and setting $\sigma_p^1 = \sigma_c^2 = \sigma^+$, $\sigma_c^1 = \sigma_p^2 = \sigma^-$, we can produce two polarization-entangled Bell states

$$|\Psi^{\pm}\rangle = \frac{1}{\sqrt{2}}\left(\left|\sigma_s^+\sigma_{as}^-\right\rangle \pm \left|\sigma_s^-\sigma_{as}^+\right\rangle\right). \quad (3)$$

Similarly, by setting $\sigma_p^1 = \sigma_c^1 = \sigma^+$, $\sigma_p^2 = \sigma_p^2 = \sigma^-$, we obtain other two Bell states:

$$|\Phi^{\pm}\rangle = \frac{1}{\sqrt{2}}\left(\left|\sigma_s^+\sigma_{as}^+\right\rangle \pm \left|\sigma_s^-\sigma_{as}^-\right\rangle\right). \quad (4)$$

Figure 3 displays the measured two-photon polarization correlations for $|\Psi^+\rangle$ by locking $\phi = 0$. The coincidence counts are integrated from τ = 15 to 50 ns for a total measurement time of 60 s. The circle data (○, red) are collected by fixing the Stokes photon polarization angle at 0° and the triangle data (△, blue) at −45°. Other parameters during the measurement remain the same as those for Fig. 2(c). The solid cosine- and sine-wave curves are the theoretical fits with adjustable background and amplitude parameters. We obtain the visibility V = 89.7%, which is beyond the requirement

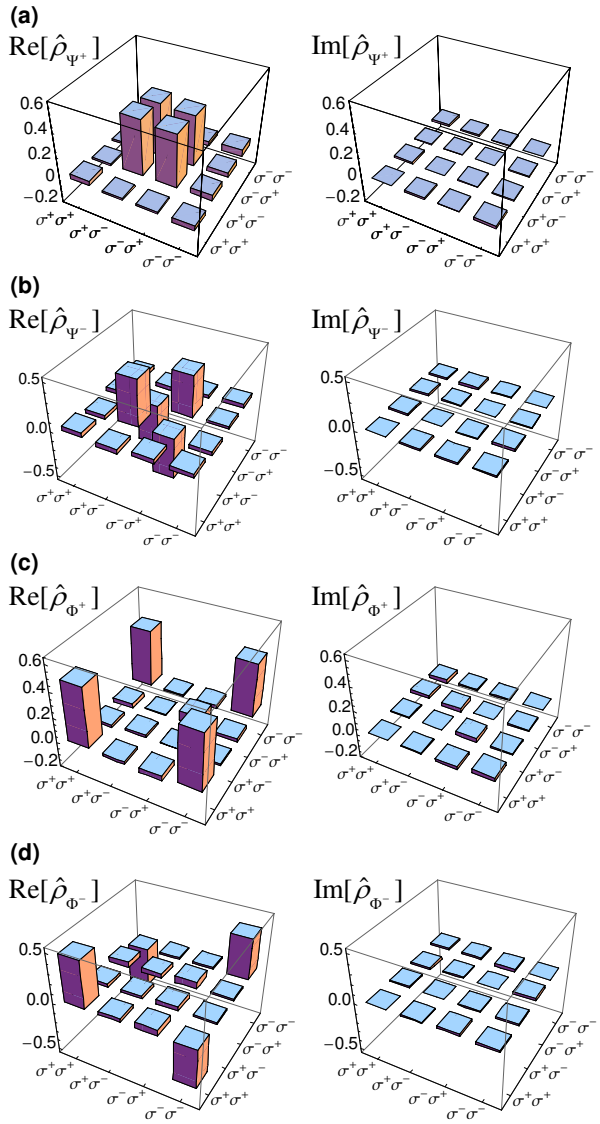

FIG. 4: (color online). Tomography measurement results of the photon pairs at the target polarization entangled Bell states (a) $|\Psi^+\rangle$, (b) $|\Psi^-\rangle$, (c) $|\Phi^+\rangle$, and (d) $|\Phi^-\rangle$.

of $1/\sqrt{2}$ for violating the Bell-CHSH inequality[20]. For comparison, we plot the data without locking the phase as the square points (□, black) which shows no quantum interference.

To obtain a complete characterization of the polarization entanglement, we also make a quantum state tomography to determine the density matrix following the maximum likelihood estimation method [21, 22]. With two additional quarter-wave plates, the circular polarization basis $|\sigma_s^+\sigma_{as}^-\rangle$,$|\sigma_s^-\sigma_{as}^+\rangle$,$|\sigma_s^+\sigma_{as}^+\rangle$ and $|\sigma_s^-\sigma_{as}^-\rangle$ can be converted into linear polarization basis $|HH\rangle$,$|VV\rangle$,$|HV\rangle$ and $|VH\rangle$. Then we use a half-wave plate followed by a PBS as the polarization selector. The density matrix is constructed from the coincidence counts at 16 independent projection states [See the supplementary material [19]]. The graphical representation of the obtained density matrix for $|\Psi^\pm\rangle$ and $|\Phi^\pm\rangle$ are shown in Fig. 4, and from which we obtain the fidelities of 93.8%, 95.7% , 91.6%, and 92.4%, respectively. We also use the density matrix to test the violation of Bell-CHSH inequality ($S > 2$) and get the value $S = 2.53 \pm 0.02$, 2.54 ± 0.02, 2.414 ± 0.037, and 2.16 ± 0.041 for the obtained four Bell states.

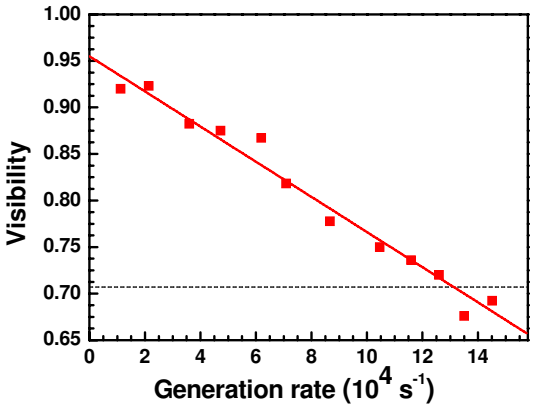

FIG. 5: (color online). Visibility versus the biphoton generation rate. The solid line is linear fit. The dashed line marks the boundary for violating the Bell-CHSH inequality.

Now, we turn to the brightness of our photon source. For the data shown in Fig. 2 (c), taking into account the fiber coupling efficiency (70%), filter transmission (70%), detector quantum efficiency (50%) and duty cycle (10%), our photon source spontaneously generate about 70000 photon pairs per second. With the pump power of 70 μW and a linewidth of 2.9 MHz, we estimate a spectrum brightness of 24000 s^{-1}MHz^{-1} and the normalized spectrum brightness of 344000 s^{-1}MHz^{-1} mW^{-1}. As compared with that of the recent cavity-based spontaneous parametric down conversion source [8], the brightness is improved by five orders of magnitude. We can further increase the photon pair generation rate by increasing the pump laser power. Figure 5 shows the dependance of the visibility of the polarization correlation to the photon pair generation rate. The visibility is estimated from $V = (g^{(2)}_{s,as} - 1)/(g^{(2)}_{s,as} + 1)$ [23, 24]. As long as the generation rate is less than 1.3×10^5 s^{-1}, the visibility is larger than $1/\sqrt{2}$, which is the boundary to violate the Bell-CHSH inequality.

In summary, we have demonstrated an efficient experimental scheme for producing subnatural-linewidth photon pairs with entanglements in both continuous time-frequency domain and discrete polarizations. The polarization entanglement results from the interference between the two SFWM spatial paths. By stabilizing the phase difference between these two paths and setting

properly the driving laser polarizations, we produce all four Bell states, confirmed by the quantum state tomography measurements. Their long coherence time (up to 900 ns) and narrow bandwidth (about 1 MHz) make them a promising entangled photon source that interact with rubidium atomic quantum nodes.

We thank JF Chen and C Liu for their helpful discussion. This work was supported by the NSFC (Grant Nos. 11104085, 11125417 and 61378012), the Major Research Plan of the NSFC (Grant No. 91121023), the SKPBR of China (Grant Nos. 2011CBA00200 and 2013CB921804), and the PCSIRT(Grant No. IRT1243). S.D. was support by Hong Kong Research Grants Council (Project No. HKU8/CRF/11G).

* Electronic address: yanhui@scnu.edu.cn
† Electronic address: slzhunju@163.com

[1] L. M. Duan, M. D. Lukin, J. I. Cirac, and P. Zoller, Nature (London) **414**, 413 (2001).
[2] H. J. Kimble, Nature (London) **453**, 1023 (2008).
[3] J. T. Barreiro, N. K. Langford, N. A. Peters, and P. G. Kwiat, Phys. Rev. Lett. **95**, 260501 (2005).
[4] J. Chen, J. Fan, M. D. Eisaman, and A. Migdall, Phys. Rev. A **77**, 053812 (2008).
[5] R. Ceccarelli, G. Vallone, F. De Martini, P. Mataloni, and A. Cabello, Phys. Rev. Lett. **103**, 160401 (2009).
[6] Z. Y. Ou, and Y. J. Lu, Phys. Rev. Lett. **83**, 2556 (1999).
[7] H. Wang, T. Horikiri, and T. Kobayashi, Phys. Rev. A **70**, 043804 (2004).
[8] X. H. Bao, Y. Qian, J. Yang, H. Zhang, Z.-B. Chen, T. Yang, and J.-W. Pan, Phys. Rev. Lett. **101**, 190501 (2008).
[9] H. Zhang, X. M. Jin, J. Yang, H. N. Dai, S. J. Yang, T. M. Zhao, J. Rui, Y. He, X. Jiang, F. Yang, G. S. Pan, Z. S. Yuan, Y. Deng, Z. B. Chen, X. H. Bao, S. Chen, B. Zhao, and J. W. Pan, Nat. Photonics **5**, 628 (2011).
[10] S. W. Du, P. Kolchin, C. Belthangady, G. Y. Yin, and S. E. Harris, Phys. Rev. Lett. **100**, 183603 (2008).
[11] S. W. Du, J. M. Wen, and M. H. Rubin, J. Opt. Soc. Am. B **25**, C98 (2008).
[12] S. Y. Zhou, S. C. Zhang, C. Liu, J. F. Chen, J. M. Wen, M. M. T. Loy, G. K. L. Wong, and S. W. Du, Opt. Express **22**, 24124 (2012).
[13] S. Zhang, J. F. Chen, C. Liu, M. M. T. Loy, G. K. L. Wong, and S. Du, Phys. Rev. Lett. **106**, 243602 (2011).
[14] S. Zhang, C. Liu, S. Zhou, C.-S. Chuu, M. M. T. Loy, and S. Du, Phys. Rev. Lett. **109**, 263601 (2012).
[15] Y. C. Chen, C. W. Lin, and I. A. Yu, Phys. Rev. A **61**, 053805 (2000).
[16] H. Yan, S. C. Zhang, J. F. Chen, M. M. T. Loy, G. K. L. Wong, and S. W. Du, Phys. Rev. Lett. **106**, 033601 (2011).
[17] D. Matsukevich and A. Kuzmich, Science **306**, 663 (2004).
[18] S. Zhang, J. F. Chen, C. Liu, S. Zhou, M. M. T. Loy, G. K. L. Wong, and S. Du, Rev. Sci. Instrum. **83**, 073102 (2012).
[19] See Supplemental Material for the derivation of Eq. (1) and Eq. (2), the method to lock the phase ϕ, and the density matrix results of the four Bell states.
[20] J. F. Clauser, Phys. Rev. D. **9**, 853 (1974).
[21] A. G. White, D. F. V. James, P. H. Eberhard, and P. G. Kwiat, Phys. Rev. Lett. **83**, 3103 (1999).
[22] D. F. V. James, P. G. Kwiat, W. J. Munro, and A. G. White, Phys. Rev. A **64**, 052312 (2001).
[23] H. de Riedmatten, J. Laurat, C. W. Chou, E. W. Schomburg, D. Felinto, and H. J. Kimble, Phys. Rev. Lett. **97**, 113603 (2006).
[24] J. K. Thompson, J. Simon, H. Q. Loh, and V. Vuletić, Science **313**, 74 (2006).
[25] J. M. Wen and M. H. Rubin, Phys. Rev. A **74**, 023808(2006).
[26] J. M. Wen and M. H. Rubin, Phys. Rev. A **74**, 023809(2006).

Supplemental Material:

DERIVATION OF EQS. (1) AND (2)

In the interaction picture the effective interaction Hamiltonian for the four-wave mixing (FWM) parametric process takes the form[11, 25, 26]

$$\begin{aligned}\hat{H}_I(t) &= \frac{i\hbar L}{2\pi}\int d\omega_{as}d\omega_s\kappa\mathrm{sinc}(\frac{\Delta kL}{2})\frac{1}{\sqrt{2}}[\hat{a}^+_{\sigma_p^1}(\omega_s)\hat{a}^+_{\sigma_c^1}(\omega_{as})+\hat{a}^+_{\sigma_p^2}(\omega_s)\hat{a}^+_{\sigma_c^2}(\omega_{as})e^{ik_c(L_{c2}-L_{c1})}e^{ik_p(L_{p2}-L_{p1})}]\\ &\cdot e^{-i(\omega_p+\omega_c-\omega_{as}-\omega_s)t}+H.C.,\\ &= \frac{i\hbar L}{2\pi}\int d\omega_{as}d\omega_s\kappa\mathrm{sinc}(\frac{\Delta kL}{2})\frac{1}{\sqrt{2}}[\hat{a}^+_{\sigma_p^1}(\omega_s)\hat{a}^+_{\sigma_c^1}(\omega_{as})+\hat{a}^+_{\sigma_p^2}(\omega_s)\hat{a}^+_{\sigma_c^2}(\omega_{as})e^{i\phi_1}e^{i\phi_2}]e^{-i(\omega_p+\omega_c-\omega_{as}-\omega_s)t}+H.C.\end{aligned} \tag{S.1}$$

where $\hat{a}^+_{\sigma_p^j}(\omega_s)$ $(j=1,2)$ is the creation operator of the Stokes photons with pump polarization σ_p^j, $\hat{a}^+_{\sigma_c^j}(\omega_{as})$ $(j=1,2)$ is the creation operator of the anti-Stokes photons with coupling polarization σ_c^j, L_{c_j} (L_{p_j}) is the length of the coupling (pump) laser arm j in the Mach-Zehnder interferometer, $\phi_1=k_c(L_{c2}-L_{c1})$, $\phi_2=k_p(L_{p2}-L_{p1})$. Based on perturbation theory [11], the two-photon (biphoton) state $|\Psi\rangle$ can be expressed as

$$\begin{aligned}|\Psi\rangle &= -\frac{i}{\hbar}\int_{-\infty}^{+\infty}dt\hat{H}_I(t)|0\rangle\\ &= L\int d\omega_{as}\kappa(\omega_{as})\mathrm{sinc}(\frac{\Delta k(\omega_{as})L}{2})\frac{1}{\sqrt{2}}[\hat{a}^+_{\sigma_p^1}(\omega_p+\omega_c-\omega_{as})\hat{a}^+_{\sigma_c^1}(\omega_{as})+\hat{a}^+_{\sigma_p^2}(\omega_p+\omega_c-\omega_{as})\hat{a}^+_{\sigma_c^2}(\omega_{as})e^{i\phi}]|0\rangle\\ &= L\int d\omega_{as}\kappa(\omega_{as})\mathrm{sinc}(\frac{\Delta k(\omega_{as})L}{2})\frac{1}{\sqrt{2}}[|\omega_s=\omega_p+\omega_c-\omega_{as},\sigma_p^1\rangle|\omega_{as},\sigma_c^1\rangle+|\omega_s=\omega_p+\omega_c-\omega_{as},\sigma_p^2\rangle|\omega_{as},\sigma_c^2\rangle e^{i\phi}]\\ &= L\int d\omega_{as}\kappa(\omega_{as})\mathrm{sinc}[\frac{\Delta k(\omega_{as})L}{2}]|\omega_s=\omega_p+\omega_c-\omega_{as}\rangle|\omega_{as}\rangle\otimes\frac{1}{\sqrt{2}}[|\sigma_p^1\rangle_s|\sigma_c^1\rangle_{as}+e^{i\phi}|\sigma_p^2\rangle_s|\sigma_c^2\rangle_{as}],\end{aligned} \tag{S.2}$$

where $\phi=\phi_1+\phi_2$.

Equation (S.2) shows generation of both time-frequency entanglement (energy conservation due to the time translation symmetry of the system $\omega_s=\omega_c+\omega_p-\omega_{as}$) and polarization entanglement.

For simplify, Equation (S.2) can also be further described in the time and polarization domain as

$$|\Psi(t_s,t_{as})\rangle=\psi(t_{as}-t_s)e^{-i(\overline{\omega}_{as}t_{as}+\overline{\omega}_s t_s)}\otimes\frac{1}{\sqrt{2}}[|\sigma_p^1\rangle_s|\sigma_c^1\rangle_{as}+e^{i\phi}|\sigma_p^2\rangle_s|\sigma_c^2\rangle_{as}]. \tag{S.3}$$

In Eq. (S.3), the time-domain wave function $\psi(t_{as}-t_s)$, which indicates the time-frequency entanglement, is the Fourier transform of the photon spectrum $\kappa(\omega_{as})\mathrm{sinc}[\frac{\Delta k(\omega_{as})L}{2}]$ and can be measured through coincidence counts in the time domain directly. Equations (S.2) and (S.3) correspond to Eqs. (1) and (2) in the main text, respectively.

METHOD TO LOCK PHASE FACTOR ϕ

In order to produce the polarization entangled Bell state, the phase difference ϕ in Eq.(2) in the main text should be locked. For the experimental setup, the phase difference is given by

$$\phi=\frac{2\pi}{\lambda_c}(L_{c2}-L_{c1})+\frac{2\pi}{\lambda_p}(L_{p2}-L_{p1}), \tag{S.4}$$

where λ_c (λ_p) is the wave length of the coupling (pump) laser beam. Let's define

$$k_0=\frac{k_c+k_p}{2},\delta=\frac{k_c-k_p}{2}, \tag{S.5}$$

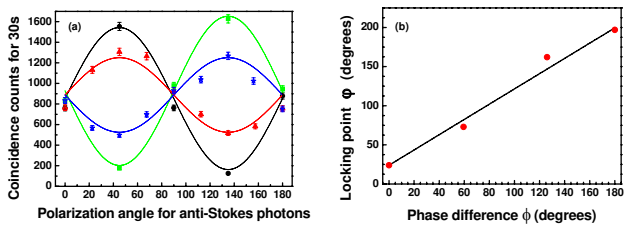

FIG. S1: (color online). (a) Polarization correlation of the paired Stokes and anti-Stokes photons. The polarization angle for Stokes photons are set at -45°, the phase difference ϕ is 0 (black line and cycle), $\pi/3$ (red line and triangle), $2\pi/3$ (blue line and star) and π (green line and square), respectively. (b)The locking point versus the phase difference of the polarization entangled state. All of the solid lines are theoretically fitted.

then the phase difference can be rewritten as

$$\phi = k_0[(L_{c2} + L_{p2}) - (L_{c1} + L_{p1})] + \delta[(L_{c2} - L_{p2}) - (L_{c1} - L_{p1})]. \tag{S.6}$$

Under the condition $k_0 \gg \delta$, Equation (S.6) can be further reduced to

$$\phi \approx k_0[(L_{c2} + L_{p2}) - (L_{c1} + L_{p1})] = \frac{k_0}{k_l}\varphi + \varphi_0, \tag{S.7}$$

here $\varphi = k_l[(L_{c2} + L_{p2}) - (L_{c1} + L_{p1})]$ is the phase difference of the Mach-Zehnder interferometer for the locking laser (k_l, 795nm), φ_0 is the phase shift between the two Mach-Zehnder interferometers (the locking laser doesn't overlap with the pump-coupling laser fields).

We use the two-photon polarization correlation measurement to determine the relation between the locking point φ and the phase difference ϕ. As shown in Fig. (S.1), with four groups of correlation measurements ($0, \pi/3, 2\pi/3$ and π), the locking point φ are found to be linearly relative to the phase difference ϕ that fitted very well with the theoretical results from Eq. (S.7).

DENSITY MATRIX RESULTS OF THE FOUR BELL STATES

The properties of the four Bell states generated in our experiments are described in the main text. The detailed density matrix results are showing in the following:

$$|\Psi^+\rangle: \begin{pmatrix} 0.041 & 0.006+0.015i & -0.023-0.004i & -0.009+0.028i \\ 0.006-0.015i & 0.454 & 0.482-0.007i & 0.084+0.011i \\ -0.023+0.004i & 0.482+0.007i & 0.427 & -0.01-0.01i \\ -0.009-0.028i & 0.084-0.011i & -0.01+0.01i & 0.078 \end{pmatrix},$$

$$|\Psi^-\rangle: \begin{pmatrix} 0.045 & -0.041+0.017i & 0.038+0.018i & 0.04-0.012i \\ -0.041-0.017i & 0.483 & -0.442+0.01i & -0.039-0.024i \\ 0.038-0.018i & -0.442-0.01i & 0.433 & 0.026-0.008i \\ 0.04+0.012i & -0.039+0.024i & 0.026+0.008i & 0.038 \end{pmatrix},$$

$$|\Phi^+\rangle: \begin{pmatrix} 0.482 & -0.062+0.023i & -0.103+0.012i & 0.48-0.013i \\ -0.062-0.023i & 0.029 & 0.032-0.048i & 0.112+0.022i \\ -0.103-0.012i & 0.032+0.048i & 0.127 & 0.019-0.047i \\ 0.48+0.013i & 0.112-0.022i & 0.019+0.047i & 0.361 \end{pmatrix},$$

$$|\Phi^-\rangle: \begin{pmatrix} 0.481 & 0.032+0.011i & 0.056-0.022i & -0.409+0.018i \\ 0.032-0.011i & 0.029 & 0.043+0.009i & 0.016+0.016i \\ 0.056+0.022i & 0.043-0.009i & 0.072 & 0.017-0.027i \\ -0.409-0.018i & 0.016-0.016i & 0.017+0.027i & 0.418 \end{pmatrix}.$$